Article

Superconducting Diode Effect in Topological Hybrid Structures

Tairzhan Karabassov [1,*], Emir S. Amirov [1], Irina V. Bobkova [2,3,4], Alexander A. Golubov [1,5], Elena A. Kazakova [6] and Andrey S. Vasenko [1,7,*]

1 School of Electronic Engineering, HSE University, 101000 Moscow, Russia
2 Institute of Solid State Physics, 142432 Chernogolovka, Russia
3 Moscow Institute of Physics and Technology, 141700 Dolgoprudny, Russia
4 Faculty of Physics, HSE University, 101000 Moscow, Russia
5 Faculty of Science and Technology and MESA+ Institute for Nanotechnology, University of Twente, 7500 AE Enschede, The Netherlands
6 Department of Biochemistry, Sechenov First Moscow State Medical University, 119991 Moscow, Russia
7 I.E. Tamm Department of Theoretical Physics, P.N. Lebedev Physical Institute, Russian Academy of Sciences, 119991 Moscow, Russia
* Correspondence: tkarabasov@hse.ru (T.K.); avasenko@hse.ru (A.S.V.)

Abstract: Currently, the superconducting diode effect (SDE) is being actively discussed, due to its large application potential in superconducting electronics. In particular, superconducting hybrid structures, based on three-dimensional (3D) topological insulators, are among the best candidates, due to their having the strongest spin–orbit coupling (SOC). Most theoretical studies on the SDE focus either on a full numerical calculation, which is often rather complicated, or on the phenomenological approach. In the present paper, we compare the linearized and nonlinear microscopic approaches in the superconductor/ferromagnet/3D topological insulator (S/F/TI) hybrid structure. Employing the quasiclassical Green's function formalism we solve the problem self-consistently. We show that the results obtained by the linearized approximation are not qualitatively different from the nonlinear solution. The main distinction in the results between the two methods was quantitative, i.e., they yielded different supercurrent amplitudes. However, when calculating the so-called diode quality factor the quantitative difference is eliminated and both approaches result in good agreement.

Keywords: superconductivity; superconducting diode effect; hybrid structures; topological insulators

1. Introduction

The field of superconducting electronics is an important area in the research and development of hybrid quantum devices with lower power consumption. Superconducting hybrid structures, consisting of a superconductor and non-superconducting material (normal metal N, ferromagnet F, etc.), operate by means of the proximity effect. This effect can be described as a leakage of the superconducting correlations into the adjacent non-superconducting layer [1–11]. Superconductor/ferromagnet (S/F) structures have been proposed in many nanoelectronic applications, such as the following: memory devices [12], quantum and classical logic devices [12,13], artificial neural networks [14], detectors and bolometers [15], nanorefrigerators [16,17] and spin-valves [18]. Placing two-dimensional (2D) S/F structures on the surface of a 3D topological insulator, a material with strong spin–orbit coupling, may add new functionality and create superconducting diode, see Figure 1.

The superconducting diode effect (SDE) is an active area of research because of its great application potential in the fields of superconducting electronics and spintronics. Generally, the SDE is observed in two-dimensional superconducting systems with broken inversion and time reversal symmetries [19]. While the former usually implies the presence of the spin–orbit field, the latter can be achieved by the exchange field from the ferromagnet, or by exposing the system to an external magnetic field. These conditions

allow for the possibility of superconducting helical state realization. The helical state is characterized by the order parameter modulated in the direction transverse to the field by the phase factor $\exp\left(i\boldsymbol{q_0}\cdot\boldsymbol{r}\right)$, where $\boldsymbol{q_0}$ is the Cooper pair momentum [20]. In this case, the critical supercurrents are different in the directions parallel to and anti-parallel to the momentum $\boldsymbol{q_0}$. Significant advances have been made since the experimental discovery of the diode effect by Ando et al. [21]. There have been numerous reports involving both experimental [21–27] and theoretical studies [28–36] of the SDE. Hybrid SDE devices deserve special attention [33,37,38]. In such structures, the ingredients for the SDE effect are brought together by the proximity effect. For instance, the S/F/TI hybrid structure is a promising platform for realization of the superconducting diode [38]. It should be noticed that placing the S/F structures on the surface of a 3D topological insulator leads to a number of striking phenomena of magnetoelectric nature [39–44]. Moreover, new electronic states have been predicted to appear in such structures, including magnetic monopoles [45] and Majorana fermions [46–49]. It has also been predicted that the presence of helical magnetization in the F layer leads to nonmonotonic dependence of the critical temperature on the F layer width in S/F/TI structures [50].

The majority of the existing theoretical studies on the SDE focus either on the microscopic numerical calculations [30,32,51,52] or on the phenomenological approach [29,33]. In this work, we consider both linear and nonlinear approaches to calculate the SDE in the hybrid S/F/TI structure. We use the microscopic quasiclassical Green's function formalism in the diffusive regime. We compare the results obtained by linear and nonlinear methods and discuss their ranges of applicability.
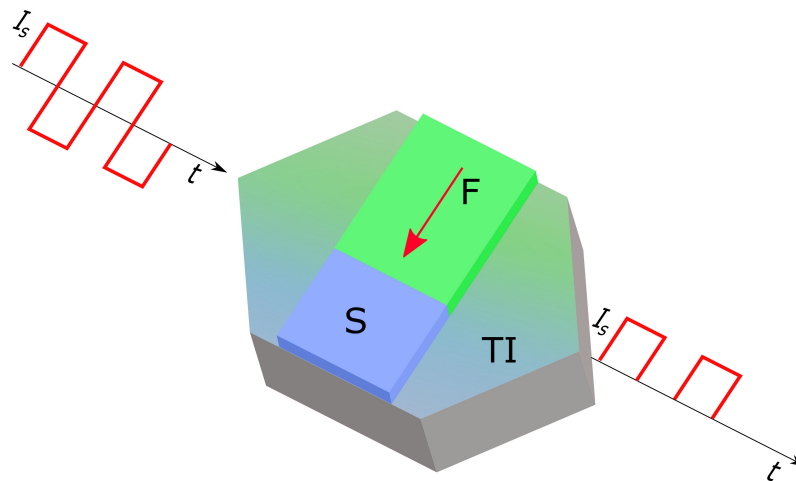

Figure 1. Schematic representation of the superconducting diode, where a two-dimensional (2D) S/F structure is placed on the surface of a three-dimensional (3D) topological insulator.

2. Materials and Methods

In this section, we present the model under consideration. The system is described by the following Hamiltonian model:

$$H = H_0 + H_F + H_S, \tag{1}$$

where

$$H_0 = \int d^2r\,\Psi^\dagger(\boldsymbol{r})\left[-i\alpha(\boldsymbol{\nabla_r}\times\hat{z})\boldsymbol{\sigma}-\mu+V(\boldsymbol{r})\right]\Psi(\boldsymbol{r}), \tag{2}$$

$$H_F = -\int d^2r\,\Psi^\dagger(\boldsymbol{r})\left[\boldsymbol{h}\boldsymbol{\sigma}\right]\Psi(\boldsymbol{r}), \tag{3}$$

$$H_S = \Delta(\boldsymbol{r})\Psi_\uparrow^\dagger(\boldsymbol{r})\Psi_\downarrow^\dagger(\boldsymbol{r}) + \Delta^*(\boldsymbol{r})\Psi_\downarrow(\boldsymbol{r})\Psi_\uparrow(\boldsymbol{r}). \tag{4}$$

Here, $\Psi^\dagger(\boldsymbol{r}) = (\Psi_\uparrow^\dagger(\boldsymbol{r}), \Psi_\downarrow^\dagger(\boldsymbol{r}))$ is the creation operator of an electron at the 3D TI surface, $\hat{z}$ is the unit vector normal to the surface of TI, α is the Fermi velocity of electrons at

the 3D TI surface and μ is the chemical potential. $\boldsymbol{\sigma} = (\sigma_x, \sigma_y, \sigma_z)$ is a vector of Pauli matrices in spin space and $\boldsymbol{h} = (h_x, h_y, 0)$ is an in-plane exchange field, which is assumed to be nonzero only at $x < 0$. The superconducting pairing potential Δ is nonzero only at $x > 0$. Therefore, effectively, the TI surface states are divided into two parts: one at $x < 0$ possesses $h \neq 0$, which can be called "ferromagnetic", while the other corresponds to $x > 0$ with $\Delta \neq 0$, which can be called "superconducting". Below we use subscripts f and s to denote quantities related to the appropriate parts of the TI surface. The potential term $V(\boldsymbol{r})$ includes the nonmagnetic impurity scattering potential $V_{imp} = \sum\limits_{\boldsymbol{r}_i} V_i \delta(\boldsymbol{r} - \boldsymbol{r}_i)$, which is of a Gaussian form $\langle V(\boldsymbol{r})V(\boldsymbol{r}')\rangle = (1/\pi\nu\tau)\delta(\boldsymbol{r} - \boldsymbol{r}')$ with $\nu = \mu/(2\pi\alpha^2)$.

The superconductivity and in-plane exchange field is assumed to be proximity-induced, due to adjacent superconducting and ferromagnetic layers. Thus, we can imagine the system as a planar hybrid structure, consisting of a superconductor, S, and a ferromagnetic layer, F, on top of a three-dimensional topological insulator, TI, as shown schematically in Figure 1. The role of the TI surface is to provide strong spin–orbit coupling which produces a full spin–momentum locking effect. In this case, only one helical band crossing the Fermi energy is present. We employ the quasiclassical Green's function formalism in the diffusive regime. In principle, Green's function matrices have two degrees of freedom that are particle–hole and spin. In our model, the spin structure is characterized by a projection onto the conduction band:

$$\check{g}_{s,f}(\boldsymbol{n}_F, \boldsymbol{r}, \varepsilon) = \hat{g}_{s,f}(\boldsymbol{r}, \varepsilon)\frac{(1 + \boldsymbol{n}_\perp \boldsymbol{\sigma})}{2}, \tag{5}$$

where, $\hat{g}_{s(f)}$ is the spinless Green's function matrix in the particle–hole space in the superconducting (ferromagnetic) part of the 3D TI layer, $\boldsymbol{n}_F = \boldsymbol{p}_F/p_F = (n_{F,x}, n_{F,y}, 0)$ is a unit vector directed along the quasiparticle trajectory and $\boldsymbol{n}_\perp = (n_{F,y}, -n_{F,x}, 0)$ is a unit vector perpendicular to the quasiparticle trajectory, and directed along the quasiparticle spin, which is locked to the quasiparticle momentum.

In our theoretical analysis, we consider the diffusive limit, in which the superconducting coherence length is given by the expression $\xi_s = \sqrt{D_s/2\pi T_{cs}}$, where D_s is the diffusion coefficient and T_{cs} is the critical temperature of the bulk superconductor (we assume $\hbar = k_B = 1$) and the elastic scattering length $\ell \ll \xi_s$. We also neglect the nonequilibrium effects in the structure [53–55].

In the following we outline the nonlinear and linear equations to calculate the SDE effect in the system under consideration.

2.1. Nonlinear Usadel Equations

The quasiclassical Usadel equation for spinless Green's functions is [56,57]:

$$D\hat{\nabla}(\hat{g}\hat{\nabla}\hat{g}) = [\omega_n \tau_z + i\hat{\Delta}, \hat{g}]. \tag{6}$$

Here, D is the diffusion constant, τ_z is the Pauli matrix in the particle–hole space, $\hat{\nabla}X = \nabla X + i(h_x \hat{e}_y - h_y \hat{e}_x)[\tau_z, \hat{g}]/\alpha$. The gap matrix $\hat{\Delta}$ is defined as $\hat{\Delta} = \hat{U}i\tau_x\Delta(x)\hat{U}^\dagger$, where $\Delta(x)$ is a real function and transformation matrix $\hat{U} = \exp(iqy\tau_z/2)$. The finite center of mass momentum q takes into account the helical state. The Green's function matrix is also transformed into $\hat{g} = \hat{U}\hat{g}_q\hat{U}^\dagger$. Inclusion of the magnetization component h_y produces no quantitative effect on either the supercurrent in y direction of the bilayer or on the critical temperature in the S part. It only enters the solution f_f as a phase factor $\exp(2ih_y x/\alpha)$ [50,56]. Thus, we did not take it into consideration in our model, and define $h_x = h$.

In the hybrid structure under consideration, the helical state appears in the system in the following way. In our system, the Zeeman field and superconducting region are spatially separated, so that the helical state is realized via the proximity effect through the S/F interface. The helical state in the system is also characterized by the order parameter with a spatially inhomogeneous phase. However, the supercurrent density is not uniform

in the structure. The total current across the hybrid structure is equal to zero. Thus, we call this state the hybrid helical state. More detailed analysis of the hybrid helical state can be found in [38].

To facilitate the solution procedures of the nonlinear Usadel equations we employ θ parametrization of the Green's functions [58]:

$$\hat{g}_q = \begin{pmatrix} \cos\theta & \sin\theta \\ \sin\theta & -\cos\theta \end{pmatrix}. \tag{7}$$

Substituting the above matrix into the Usadel Equation (6), we obtain the following in the S part of the TI surface $x > 0$:

$$\xi_s^2 \pi T_{cs} \left[\partial_x^2 \theta_s - \frac{q^2}{2} \sin 2\theta_s \right] = \omega_n \sin\theta_s - \Delta(x)\cos\theta_s,$$

and in the F part $x < 0$:

$$\xi_f^2 \pi T_{cs} \left[\partial_x^2 \theta_f - \frac{q_m^2}{2} \sin 2\theta_f \right] = \omega_n \sin\theta_f, \tag{8}$$

where $\xi_f = \sqrt{D_f/2\pi T_{cs}}$, and D_f is the diffusion coefficient of the ferromagnetic layer. $q_m = q + 2h/\alpha$ and $X_{s(f)}$ means the value of X in the S(F) part of the TI surface, respectively. The self-consistency equation for the pair potential reads:

$$\Delta(x) \ln \frac{T_{cs}}{T} = \pi T \sum_{\omega_n} \left(\frac{\Delta(x)}{|\omega_n|} - 2\sin\theta_s \right). \tag{9}$$

We supplement the above equations with the following boundary conditions at the S/F interface ($x = 0$) [59]:

$$\gamma_B \frac{\partial\theta_f}{\partial x}\bigg|_{x=0} = \sin\left(\theta_s - \theta_f\right), \tag{10}$$

$$\frac{\gamma_B}{\gamma} \frac{\partial\theta_s}{\partial x}\bigg|_{x=0} = \sin\left(\theta_s - \theta_f\right), \tag{11}$$

where $\gamma = \xi_s\sigma_f/\xi_f\sigma_s$, $\gamma_B = R\sigma_f/xi_f$, and $\sigma_{s(f)}$ is the conductivity of the S (F)layer. The parameter γ determines the strength of suppression of superconductivity in the S lead near the interface compared to the bulk. No suppression occurs for $\gamma = 0$, while strong suppression takes place for $\gamma \gg 1$. The parameter γ_B is a dimensionless parameter, describing the transparency of the S/F interface [59–61]. For example, the imperfect transparency can take place due to the Fermi velocity mismatch or presence of the potential barrier at the S/F interface. To complete the boundary problem, we also set boundary conditions at the free edges:

$$\frac{\partial\theta_f}{\partial x}\bigg|_{x=-d_f} = 0, \quad \frac{\partial\theta_s}{\partial x}\bigg|_{x=d_s} = 0. \tag{12}$$

In order to calculate the superconducting current we utilize the expression for super-current density:

$$\mathbf{J}_{s(f)} = \frac{-i\pi\sigma_{s(f)}}{4e} T \sum_{\omega_n} Tr\left[\tau_z \hat{g}_{s(f)} \hat{\nabla} \hat{g}_{s(f)} \right]. \tag{13}$$

Performing the unitary transformation U, the current density transforms as follows:

$$j_y^s(x) = -\frac{\pi \sigma_s q}{2e} T \sum_{\omega_n} \sin^2 \theta_s, \tag{14}$$

$$j_y^f(x) = -\frac{\pi \sigma_n}{2e} \left[q + \frac{2h}{\alpha} \right] T \sum_{\omega_n} \sin^2 \theta_f. \tag{15}$$

The total supercurrent flowing via the system along the y-direction can be calculated by integrating the current density of the total width of the S/F bilayer $d_f + d_s$:

$$I = \int_{-d_f}^{0} j_y^f(x) dx + \int_{0}^{d_s} j_y^s(x) dx. \tag{16}$$

2.2. Linear Usadel Equations

At the limit when $T \approx T_c$, the Usadel equations (6) can be linearized, since the normal Green's function is close to unity, i.e., $\hat{g}_q \approx \tau_z + \theta(x)\tau_x$.

In the superconducting S layer ($0 < x < d_s$), the linearized Usadel equation for the spinless amplitude θ_s reads [56–58,62]:

$$\xi_s^2 \pi T_{cs} \left(\partial_x^2 - q^2 \right) \theta_s - \omega_n \theta_s + \Delta = 0. \tag{17}$$

In the ferromagnetic region of the TI, the linearized Usadel equation takes the form:

$$\partial_x^2 \theta_f = \left[\frac{\omega_n}{\xi_f^2 \pi T_{cs}} + q_m^2 \right] \theta_f. \tag{18}$$

The solution of Equation (18) is found in the form:

$$\theta_f = C(\omega_n) \cosh k_q \left(x + d_f \right), \tag{19}$$

where

$$k_q = \sqrt{\frac{|\omega_n|}{\xi_f^2 \pi T_{cs}} + q_m^2}. \tag{20}$$

Here, $C(\omega_n)$ is found from the boundary conditions. Using boundary conditions (10), the problem is written in a closed form with respect to the Green's function f_s. At $x = 0$ the boundary conditions can be written as:

$$\xi_s \frac{\partial \theta_s(0)}{\partial x} = W^q(\omega_n) \theta_s(0), \tag{21}$$

where,

$$W^q(\omega_n) = \frac{\gamma}{\gamma_B + A_{qT}(\omega_n)}, \quad A_{qT}(\omega_n) = \frac{1}{k_q \xi_f} \coth k_q d_f. \tag{22}$$

In general, the boundary condition (21) can be complex. However, in the considered system, A_{qT} is real. Hence, the condition (21) coincides with its real-valued form.

Then, we write the self-consistency equation for Δ considering only positive Matsubara frequencies:

$$\Delta \ln \frac{T_{cs}}{T} = \pi T \sum_{\omega_n > 0} \left(\frac{2\Delta}{\omega_n} - 2\theta_s \right), \tag{23}$$

The Usadel equation in the superconducting part is given by:

$$\xi_s^2 \left(\frac{\partial^2 \theta_s}{\partial x^2} - \kappa_{qs}^2 \theta_s \right) + \frac{\Delta}{\pi T_{cs}} = 0. \tag{24}$$

Within the linearized Usadel equations, the supercurrent is also calculated in the self-consistent manner, using Equations (21)–(24).

Single-Mode Approximation

In the framework of the single-mode approximation, the solution in S is introduced in the form [63,64]:

$$\theta_s(x, \omega_n) = f(\omega_n) \cos \left(\Omega \frac{x - d_s}{\xi_s} \right), \tag{25}$$

$$\Delta(x) = \delta \cos \left(\Omega \frac{x - d_s}{\xi_s} \right). \tag{26}$$

The solution presented above automatically satisfies boundary condition (12) at $x = d_s$. Substituting expressions (25) and (26) into the Usadel equation for θ_s (24) yields:

$$f(\omega_n) = \frac{\delta}{\omega_n + \Omega^2 \pi T_{cs} + q^2 \xi_s^2 \pi T_{cs}}. \tag{27}$$

Employing the single-mode approximation and using the solution in the TI layer, as well as the boundary conditions, we find the total supercurrent flowing through the system in the y direction. We obtain the following expression:

$$I = -\frac{\pi}{4e} T \sum_{\omega_n} f^2(\omega_n) \left[\sigma_s q C_s + \frac{\sigma_n}{\beta^2} \cos^2 \left(\Omega \frac{d_s}{\xi_s} \right) q_m C_f \right], \tag{28}$$

$$C_s = \left(d_s + \frac{\xi_s}{2\Omega} \sin \left(2\Omega \frac{d_s}{\xi} \right) \right),$$

$$C_f = \left(d_f + \frac{1}{2k_q} \sinh \left(2k_q d_f \right) \right),$$

where the coefficient β is defined as:

$$\beta = \gamma_B k_q \xi_f \sinh k_q d_f + \cosh k_q d_f, \tag{29}$$

and Ω is calculated from the boundary condition for the single-mode approximation (21). In the following section, we present the results of the supercurrent calculations for both linear (self-consistent and single-mode) and nonlinear approaches.

3. Results

In this section, we present the results of the calculations based on the model presented above. For simplicity we set $\xi_s = \xi_f = \xi$.

In Figure 2, we compare $I(q)$ dependencies calculated by linear and nonlinear approaches. Both of these curves were calculated in a numerical self-consistent approach. At equilibrium, when no external supercurrent was applied, the superconducting system chose the state with non-zero q_0. This state corresponded to zero total supercurrent (in the y direction), i.e., the condition $I(q_0) = 0$ was satisfied, which can be seen in Figure 2. In the system, q cannot be varied directly, but one can apply an external supercurrent through the structure in the range between the critical supercurrents I_c^+ and I_c^-, where $I_c^{+(-)}$ is the critical supercurrent for the positive (negative) direction. Applying a certain value of the supercurrent leads to the superconducting state with a corresponding value of $q \neq q_0$. When current $|I|$ was applied in the range between I_c^+ and $|I_c^-|$ the system was still in a superconducting state for $+I$ (since there was a superconducting state with a corresponding

q), and the system was in the normal state for $-I$ (there was no superconducting state with q that corresponded to the applied current $-I$).

We noticed that the linearized solution resulted in higher values of the critical currents. As expected, the linearized approach did not capture nonlinearities in the current behavior as a function of *q*.
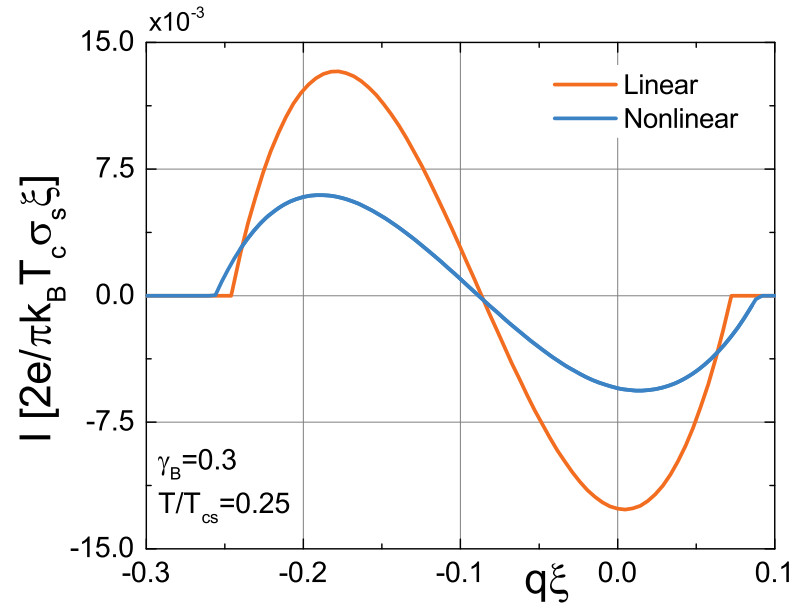

Figure 2. The total supercurrent *I* as a function of the Cooper pair momentum *q* calculated self−consistently via linear and nonlinear methods. The parameters of the calculation: $d_s = 1.2\xi$, $d_f = \xi, \gamma = 0.5, \xi h/\alpha = 0.3$.

When calculating the critical temperature in the hybrid structure, it is common to use the single-mode approach within the linearized Usadel equations. We tested the application possibility of the single-mode method in calculating the supercurrent. The main disadvantages of Equations (25) and (26) are that these expressions disregard the dependencies of the amplitude δ on the parameter *q*. Moreover, the amplitude of the pair potential cannot be obtained within the solution provided by the single-mode, i.e., δ remains as a fitting parameter. In Figure 3, we compare the full nonlinear approach and the single-mode approximation. We observed that the supercurrent derived by the single-mode was in fairly good agreement with the nonlinear method in the vicinity of the equilibrium value of $q = q_0$. However, for larger values of $q - q_0$, it was clear that the single-mode approach tended to fail, resulting in much larger values of the critical current.

In the calculations we set the temperature $T = 0.25T_{cs}$, which may seem to be out of the applicability range of the linearized Usadel equations. However, the true value of the critical temperature in the S part can be substantially lower, due to strong suppression from the adjacent F part of the structure. In our system, the critical temperature did not exceed $0.3T_c s$, as seen in Figures 2 and 3.

It is more instructive to discuss the diode quality factor, which is defined in the following way:

$$\eta = \frac{\Delta I_c}{I_c^+ + |I_c^-|} = \frac{I_c^+ - |I_c^-|}{I_c^+ + |I_c^-|}. \tag{30}$$

However, before doing so, we briefly discuss the temperature dependencies of the supercurrent nonreciprocity for the linear and nonlinear approaches. In Figure 4, the temperature dependence of $\Delta I = I_c^+ - |I_c^-|$ is demonstrated. Both methods showed approximately the same temperature when the current nonreciprocity vanished. This corresponded to the transition from the superconducting state to the normal state. It can

be seen from the figure that there was a substantial quantitative difference between the two methods.
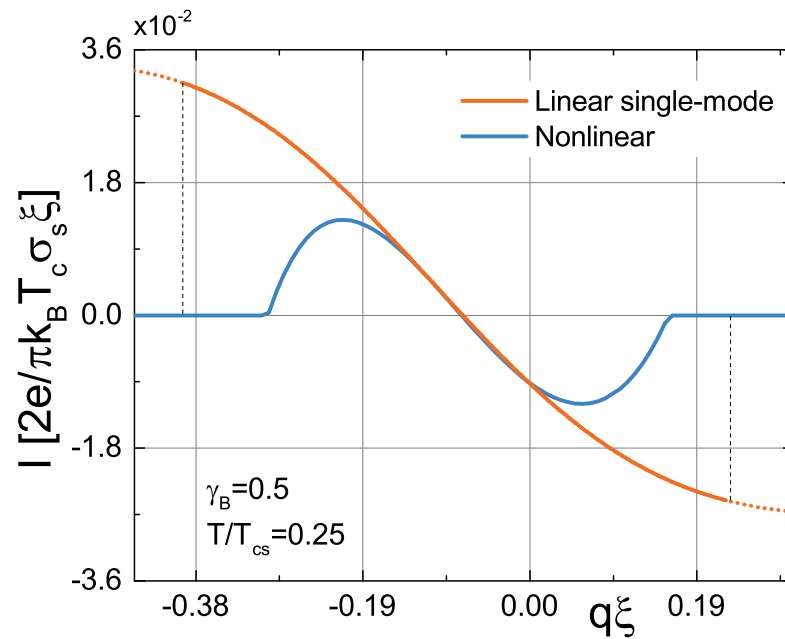

Figure 3. The total supercurrent I as a function of the Cooper pair momentum q, calculated self−consistently via linear single-mode approximation and the self-consistent nonlinear method. The amplitude of the single-mode solution $\delta = 0.05\pi T_{cs}$. The vertical dotted line corresponds to the critical temperature calculated by the single-mode approximation. The parameters of the calculation were: $d_s = 1.2\xi, d_f = \xi, \gamma = 0.5, \xi h/\alpha = 0.3$.
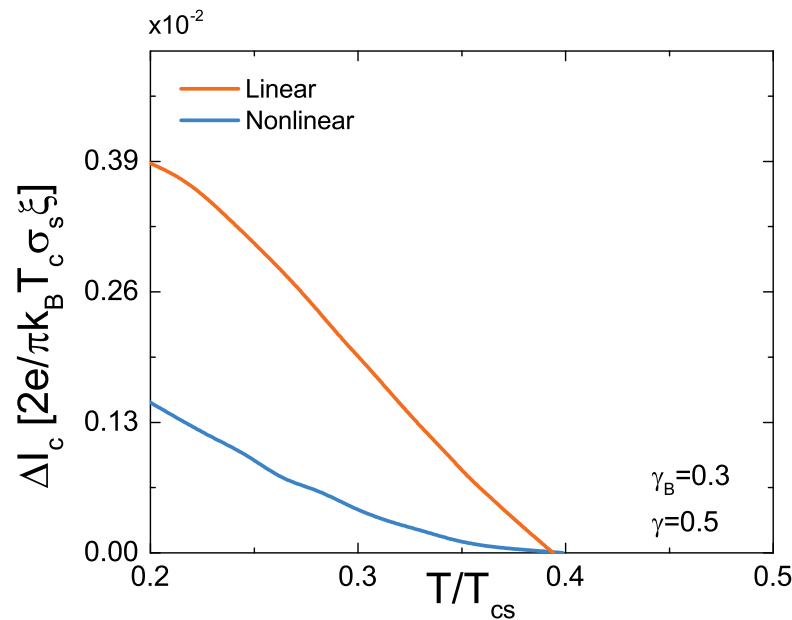
Figure 4. ΔI as a function of temperature. The parameters of the calculation were: $d_s = 1.2\xi, d_f = \xi$, $\xi h/\alpha = 0.2$.

In Figure 5, we demonstrate the SDE quality factor as a function of the exchange field $\xi h/\alpha$ for the nonlinear and linear approaches. We emphasize that the quality factors calculated for both cases were quite similar, despite the fact that $I(q)$ may be substantially different both quantitatively and qualitatively (Figure 2). This fact can be connected with the definition of the quality factor η. In brief, since η is defined as a ratio between a sum

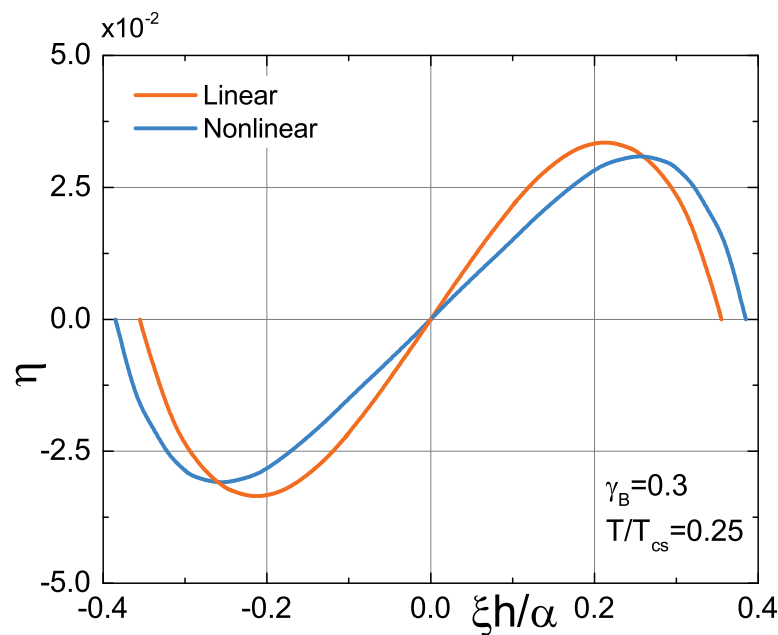and a difference of the critical currents, it loses information about current values and q dependencies.

Figure 5. SDE quality factor η as a function of exchange field h. The parameters of the calculation were: $d_s = 1.2\xi, d_f = \xi, \gamma = 0.5$.

4. Discussion

In this work, we calculated the superconducting diode effect using three different methods, which included linear and nonlinear equations.The results obtained above suggest several conclusions. The simplified single-mode approximation for the linearized Usadel equation is only applicable for a qualitative critical temperature calculation. Although the single-mode approach may be used at the vicinity of $(q - q_0)$, it does not capture the possible q dependency of the pair potential and fails at larger $|q - q_0|$. When operating close to the critical temperature, the full solution of the linearized Usadel equation provides adequate results. In particular, η, calculated via the linearized approach, is in good agreement with the nonlinear case (Figure 5). Nevertheless, in order to get a valid description of the helical state and the SDE in a wide range of parameters one should use fully nonlinear equations.

Conflicts of Interest: The authors declare no conflict of interest.

Abbreviations

The following abbreviations are used in this manuscript:

SDE   Superconducting diode effect
SOC   Spin–orbit coupling
S   Superconductor
F   Ferromagnetic material
TI   Topological insulator

References

1. Buzdin, A.I. Proximity effects in superconductor-ferromagnet heterostructures. *Rev. Mod. Phys.* **2005**, *77*, 935–976. [CrossRef]
2. Golubov, A.A.; Kupriyanov, M.Y.; Il'ichev, E. The current-phase relation in Josephson junctions. *Rev. Mod. Phys.* **2004**, *76*, 411–469. [CrossRef]
3. Bergeret, F.S.; Volkov, A.F.; Efetov, K.B. Odd triplet superconductivity and related phenomena in superconductor-ferromagnet structures. *Rev. Mod. Phys.* **2005**, *77*, 1321–1373. [CrossRef]
4. Demler, E.A.; Arnold, G.B.; Beasley, M.R. Superconducting proximity effects in magnetic metals. *Phys. Rev. B* **1997**, *55*, 15174–15182. [CrossRef]
5. Ozaeta, A.; Vasenko, A.S.; Hekking, F.W.J.; Bergeret, F.S. Andreev current enhancement and subgap conductance of superconducting *SFN* hybrid structures in the presence of a small spin-splitting magnetic field. *Phys. Rev. B* **2012**, *86*, 060509. [CrossRef]
6. Bergeret, F.S.; Tokatly, I.V. Singlet-Triplet Conversion and the Long-Range Proximity Effect in Superconductor-Ferromagnet Structures with Generic Spin Dependent Fields. *Phys. Rev. Lett.* **2013**, *110*, 117003. [CrossRef]
7. Fu, L.; Kane, C.L. Superconducting Proximity Effect and Majorana Fermions at the Surface of a Topological Insulator. *Phys. Rev. Lett.* **2008**, *100*, 096407. [CrossRef]
8. Stanescu, T.D.; Sau, J.D.; Lutchyn, R.M.; Das Sarma, S. Proximity effect at the superconductor–topological insulator interface. *Phys. Rev. B* **2010**, *81*, 241310. [CrossRef]
9. Black-Schaffer, A.M. Self-consistent superconducting proximity effect at the quantum spin Hall edge. *Phys. Rev. B* **2011**, *83*, 060504. [CrossRef]
10. Yano, R.; Hirose, H.T.; Tsumura, K.; Yamamoto, S.; Koyanagi, M.; Kanou, M.; Kashiwaya, H.; Sasagawa, T.; Kashiwaya, S. Proximity-Induced Superconducting States of Magnetically Doped 3D Topological Insulators with High Bulk Insulation. *Condens. Matter* **2019**, *4*, 9. [CrossRef]
11. Romano, P.; Polcari, A.; Cirillo, C.; Attanasio, C. Drag Voltages in a Superconductor/Insulator/Ferromagnet Trilayer. *Materials* **2021**, *14*, 7575. [CrossRef] [PubMed]
12. Soloviev, I.I.; Klenov, N.V.; Bakurskiy, S.V.; Kupriyanov, M.Y.; Gudkov, A.L.; Sidorenko, A.S. Beyond Moore's technologies: Operation principles of a superconductor alternative. *Beilstein J. Nanotechnol.* **2017**, *8*, 2689–2710. [CrossRef] [PubMed]
13. Chernodub, M.N.; Garaud, J.; Kharzeev, D.E. Chiral Magnetic Josephson Junction as a Base for Low-Noise Superconducting Qubits. *Universe* **2022**, *8*, 657. [CrossRef]
14. Soloviev, I.I.; Schegolev, A.E.; Klenov, N.V.; Bakurskiy, S.V.; Kupriyanov, M.Y.; Tereshonok, M.V.; Shadrin, A.V.; Stolyarov, V.S.; Golubov, A.A. Adiabatic superconducting artificial neural network: Basic cells. *J. Appl. Phys.* **2018**, *124*, 152113. [CrossRef]
15. Gordeeva, A.V.; Pankratov, A.L.; Pugach, N.G.; Vasenko, A.S.; Zbrozhek, V.O.; Blagodatkin, A.V.; Pimanov, D.A.; Kuzmin, L.S. Record electron self-cooling in cold-electron bolometers with a hybrid superconductor-ferromagnetic nanoabsorber and traps. *Sci. Rep.* **2020**, *10*, 21961. [CrossRef]
16. Ozaeta, A.; Vasenko, A.S.; Hekking, F.W.J.; Bergeret, F.S. Electron cooling in diffusive normal metal–superconductor tunnel junctions with a spin-valve ferromagnetic interlayer. *Phys. Rev. B* **2012**, *85*, 174518. [CrossRef]
17. Kawabata, S.; Ozaeta, A.; Vasenko, A.S.; Hekking, F.W.; Bergeret, F.S. Efficient electron refrigeration using superconductor/spin-filter devices. *Appl. Phys. Lett.* **2013**, *103*, 032602. [CrossRef]
18. Neilo, A.; Bakurskiy, S.; Klenov, N.; Soloviev, I.; Kupriyanov, M. Superconducting Valve Exploiting Interplay between Spin-Orbit and Exchange Interactions. *Nanomaterials* **2022**, *12*, 4426. [CrossRef] [PubMed]
19. Nadeem, M.; Fuhrer, M.S.; Wang, X. Superconducting Diode Effect–Fundamental Concepts, Material Aspects, and Device Prospects. *arXiv* **2023**, arXiv:2301.13564.
20. Houzet, M.; Meyer, J.S. Quasiclassical theory of disordered Rashba superconductors. *Phys. Rev. B* **2015**, *92*, 014509. [CrossRef]
21. Ando, F.; Miyasaka, Y.; Li, T.; Ishizuka, J.; Arakawa, T.; Shiota, Y.; Moriyama, T.; Yanase, Y.; Ono, T. Observation of superconducting diode effect. *Nature* **2020**, *584*, 373–376. [CrossRef] [PubMed]
22. Bauriedl, L.; Bäuml, C.; Fuchs, L.; Baumgartner, C.; Paulik, N.; Bauer, J.M.; Lin, K.Q.; Lupton, J.M.; Taniguchi, T.; Watanabe, K.; et al. Supercurrent diode effect and magnetochiral anisotropy in few-layer NbSe2. *Nat. Commun.* **2022**, *13*, 4266. [CrossRef] [PubMed]

23. Shin, J.; Son, S.; Yun, J.; Park, G.; Zhang, K.; Shin, Y.J.; Park, J.G.; Kim, D. Magnetic proximity-induced superconducting diode effect and infinite magnetoresistance in van der waals heterostructure. *arXiv* **2021**, arXiv:2111.05627.

24. Trahms, M.; Melischek, L.; Steiner, J.F.; Mahendru, B.; Tamir, I.; Bogdanoff, N.; Peters, O.; Reecht, G.; Winkelmann, C.B.; von Oppen, F.; et al. Diode effect in Josephson junctions with a single magnetic atom. *arXiv* **2022**, arXiv:2212.04432.

25. Chahid, S.; Teknowijoyo, S.; Mowgood, I.; Gulian, A. High-frequency diode effect in superconducting Nb$_3$Sn microbridges. *Phys. Rev. B* **2023**, *107*, 054506. [CrossRef]

26. Chahid, S.; Teknowijoyo, S.; Gulian, A. Quadristor: A novel device for superconducting electronics. *arXiv* **2022**, arXiv:2211.13340.

27. Suri, D.; Kamra, A.; Meier, T.N.G.; Kronseder, M.; Belzig, W.; Back, C.H.; Strunk, C. Non-reciprocity of vortex-limited critical current in conventional superconducting micro-bridges. *Appl. Phys. Lett.* **2022**, *121*, 102601. .. [CrossRef]

28. Daido, A.; Ikeda, Y.; Yanase, Y. Intrinsic Superconducting Diode Effect. *Phys. Rev. Lett.* **2022**, *128*, 037001. [CrossRef]

29. He, J.J.; Tanaka, Y.; Nagaosa, N. A phenomenological theory of superconductor diodes. *New J. Phys.* **2022**, *24*, 053014. [CrossRef]

30. Yuan, N.F.Q.; Fu, L. Supercurrent diode effect and finite-momentum superconductors. *Proc. Natl. Acad. Sci. USA* **2022**, *119*, e2119548119. [CrossRef]

31. Scammell, H.D.; Li, J.I.A.; Scheurer, M.S. Theory of zero-field superconducting diode effect in twisted trilayer graphene. *2D Mater.* **2022**, *9*, 025027. [CrossRef]

32. Ilić, S.; Bergeret, F.S. Theory of the Supercurrent Diode Effect in Rashba Superconductors with Arbitrary Disorder. *Phys. Rev. Lett.* **2022**, *128*, 177001. [CrossRef]

33. Devizorova, Z.; Putilov, A.V.; Chaykin, I.; Mironov, S.; Buzdin, A.I. Phase transitions in superconductor/ferromagnet bilayer driven by spontaneous supercurrents. *Phys. Rev. B* **2021**, *103*, 064504. [CrossRef]

34. de Picoli, T.; Blood, Z.; Lyanda-Geller, Y.; Väyrynen, J.I. Superconducting diode effect in quasi-one-dimensional systems. *arXiv* **2023**, arXiv:2302.04277.

35. Grein, R.; Eschrig, M.; Metalidis, G.; Schön, G. Spin-Dependent Cooper Pair Phase and Pure Spin Supercurrents in Strongly Polarized Ferromagnets. *Phys. Rev. Lett.* **2009**, *102*, 227005. [CrossRef] [PubMed]

36. Lu, B.; Ikegaya, S.; Burset, P.; Tanaka, Y.; Nagaosa, N. Tunable Josephson diode effect on the surface of topological insulators. *arXiv* **2023**, arXiv:2211.10572.

37. Kokkeler, T.H.; Golubov, A.A.; Bergeret, F.S. Field-free anomalous junction and superconducting diode effect in spin-split superconductor/topological insulator junctions. *Phys. Rev. B* **2022**, *106*, 214504. [CrossRef]

38. Karabassov, T.; Bobkova, I.V.; Golubov, A.A.; Vasenko, A.S. Hybrid helical state and superconducting diode effect in superconductor/ferromagnet/topological insulator heterostructures. *Phys. Rev. B* **2022**, *106*, 224509. [CrossRef]

39. Bobkova, I.V.; Barash, Y.S. Effects of spin-orbit interaction on superconductor-ferromagnet heterostructures: Spontaneous electric and spin surface currents. *J. Exp. Theor. Phys. Lett.* **2004**, *80*, 494–499. [CrossRef]

40. Mironov, S.; Buzdin, A. Spontaneous Currents in Superconducting Systems with Strong Spin-Orbit Coupling. *Phys. Rev. Lett.* **2017**, *118*, 077001. [CrossRef]

41. Pershoguba, S.S.; Björnson, K.; Black-Schaffer, A.M.; Balatsky, A.V. Currents Induced by Magnetic Impurities in Superconductors with Spin-Orbit Coupling. *Phys. Rev. Lett.* **2015**, *115*, 116602. [CrossRef] [PubMed]

42. Mal'shukov, A.G. Fraunhofer oscillations of the critical current at a varying Zeeman field in a spin-orbit coupled Josephson junction. *Phys. Rev. B* **2020**, *102*, 134509. [CrossRef]

43. Mal'shukov, A.G. Spontaneous generation of vortices by a nonuniform Zeeman field in a two-dimensional Rashba-coupled superconductor. *Phys. Rev. B* **2020**, *102*, 144503. [CrossRef]

44. Mal'shukov, A.G. Supercurrent vortices and Majorana zero modes induced by an in-plane Zeeman field on the surface of a three-dimensional topological insulator. *Phys. Rev. B* **2020**, *101*, 134514. [CrossRef]

45. Qi, X.L.; Li, R.; Zang, J.; Zhang, S.C. Inducing a Magnetic Monopole with Topological Surface States. *Science* **2009**, *323*, 1184–1187. [CrossRef]

46. Tanaka, Y.; Yokoyama, T.; Nagaosa, N. Manipulation of the Majorana Fermion, Andreev Reflection, and Josephson Current on Topological Insulators. *Phys. Rev. Lett.* **2009**, *103*, 107002. [CrossRef]

47. Maiellaro, A.; Citro, R. Topological Edge States of a Majorana BBH Model. *Condens. Matter* **2021**, *6*, 15. [CrossRef]

48. Mazziotti, M.V.; Scopigno, N.; Grilli, M.; Caprara, S. Majorana Fermions in One-Dimensional Structures at LaAlO$_3$/SrTiO$_3$ Oxide Interfaces. *Condens. Matter* **2018**, *3*, 37. [CrossRef]

49. Maiellaro, A.; Illuminati, F.; Citro, R. Topological Phases of an Interacting Majorana Benalcazar–Bernevig–Hughes Model. *Condens. Matter* **2022**, *7*, 26. [CrossRef]

50. Karabassov, T.; Golubov, A.A.; Silkin, V.M.; Stolyarov, V.S.; Vasenko, A.S. Reentrant superconductivity in proximity to a topological insulator. *Phys. Rev. B* **2021**, *103*, 224508. [CrossRef]

51. Legg, H.F.; Loss, D.; Klinovaja, J. Superconducting diode effect due to magnetochiral anisotropy in topological insulators and Rashba nanowires. *Phys. Rev. B* **2022**, *106*, 104501. [CrossRef]

52. Davydova, M.; Prembabu, S.; Fu, L. Universal Josephson diode effect. *Sci. Adv.* **2022**, *8*, 309. . [CrossRef]

53. Vasenko, A.S.; Hekking, F.W. Nonequilibrium electron cooling by NIS tunnel junctions. *J. Low Temp. Phys.* **2009**, *154*, 221–232. [CrossRef]

54. Arutyunov, K.Y.; Auraneva, H.P.; Vasenko, A.S. Spatially resolved measurement of nonequilibrium quasiparticle relaxation in superconducting Al. *Phys. Rev. B* **2011**, *83*, 104509. [CrossRef]

55.　Arutyunov, K.Y.; Chernyaev, S.A.; Karabassov, T.; Lvov, D.S.; Stolyarov, V.S.; Vasenko, A.S. Relaxation of nonequilibrium quasiparticles in mesoscopic size superconductors. *J. Phys. Condens. Matter* **2018**, *30*, 343001. [CrossRef]

56.　Zyuzin, A.; Alidoust, M.; Loss, D. Josephson junction through a disordered topological insulator with helical magnetization. *Phys. Rev. B* **2016**, *93*, 214502. [CrossRef]

57.　Bobkova, I.V.; Bobkov, A.M. Electrically controllable spin filtering based on superconducting helical states. *Phys. Rev. B* **2017**, *96*, 224505. [CrossRef]

58.　Belzig, W.; Wilhelm, F.K.; Bruder, C.; Schön, G.; Zaikin, A.D. Quasiclassical Green's function approach to mesoscopic superconductivity. *Superlattices Microstruct.* **1999**, *25*, 1251–1288. [CrossRef]

59.　Kuprianov, M.Y.; Lukichev, V.F. Influence of boundary transparency on the critical current of "dirty" SS'S structures. *J. Exp. Theor. Phys. Lett.* **1988**, *67*, 1163.

60.　Bezuglyi, E.V.; Vasenko, A.S.; Shumeiko, V.S.; Wendin, G. Nonequilibrium effects in tunnel Josephson junctions. *Phys. Rev. B* **2005**, *72*, 014501. [CrossRef]

61.　Bezuglyi, E.V.; Vasenko, A.S.; Bratus, E.N.; Shumeiko, V.S.; Wendin, G. Subgap current in superconducting tunnel junctions with diffusive electrodes. *Phys. Rev. B* **2006**, *73*, 220506. [CrossRef]

62.　Usadel, K.D. Generalized Diffusion Equation for Superconducting Alloys. *Phys. Rev. Lett.* **1970**, *25*, 507–509. [CrossRef]

63.　Fominov, Y.V.; Chtchelkatchev, N.M.; Golubov, A.A. Nonmonotonic critical temperature in superconductor/ferromagnet bilayers. *Phys. Rev. B* **2002**, *66*, 014507. [CrossRef]

64.　Karabassov, T.; Stolyarov, V.S.; Golubov, A.A.; Silkin, V.M.; Bayazitov, V.M.; Lvov, B.G.; Vasenko, A.S. Competitive 0 and π states in S/F/S trilayers: Multimode approach. *Phys. Rev. B* **2019**, *100*, 104502. [CrossRef]